PRAMANA
— journal of
physics



Vol. 72, No. 2
February 2009
pp. 363–373

# Reaction mechanism study of $^{7}$Li($^{7}$Li,$^{6}$He) reaction at above Coulomb barrier energies

V V PARKAR*, V JHA, S SANTRA, B J ROY, K RAMACHANDRAN, A SHRIVASTAVA, K MAHATA, A CHATTERJEE and S KAILAS
Nuclear Physics Division, Bhabha Atomic Research Centre, Mumbai 400 085, India
*Corresponding author. E-mail: parkarvivek@rediffmail.com

MS received 6 June 2008; accepted 20 August 2008

**Abstract.** The elastic scattering and the $^{6}$He angular distributions were measured in $^{7}$Li + $^{7}$Li reaction at two energies, $E_{\rm lab}$ = 20 and 25 MeV. FRDWBA calculations have been performed to explain the measured $^{6}$He data. The calculations were very sensitive to the choice of the optical model potentials in entrance and exit channels. The one-step proton transfer was found to be the dominant reaction mechanism in $^{6}$He production.

**Keywords.** $^{7}$Li($^{7}$Li,$^{6}$He) reaction; $E_{\rm lab}$ = 20 and 25 MeV; measured $\sigma(\theta)$; DWBA and CRC analysis.

**PACS Nos 25.70.Hi; 24.50.+g; 24.10.Eq**

## 1. Introduction

There have been several studies aimed at understanding the interactions between lithium nuclei at energies close to and far above the Coulomb barrier [1–6]. Reactions between these nuclei are very complex, since a variety of reaction mechanisms are competing. Compound nucleus formation was found to be dominant through the study of various exit channels for the system $^{6}$Li + $^{6}$Li [1–3], whereas both direct and compound nucleus mechanisms were found to be present for $^{7}$Li($^{7}$Li, $t/\alpha$) [4]. In the present work, we have concentrated on $^{7}$Li($^{7}$Li,$^{6}$He) reaction channel to understand the reaction mechanism.

Since the outgoing $^{6}$He in this reaction is a loosely bound unstable nucleus, it would be interesting to explore the possibility of producing it through the $^{7}$Li($^{7}$Li,$^{6}$He) reaction. The large positive $Q$ value ($Q$ = +7.279 MeV) of this reaction can be exploited in separating $^{6}$He from other reaction products and initiating further secondary reactions. A number of experiments have been reported using the low energy $^{6}$He beams [7–10] in recent times. The ($^{7}$Li,$^{6}$He) reaction on various targets was also used in the past [11–15] to extract the spectroscopic information.

However, a good understanding of the reaction mechanism is necessary in order to make use of this reaction as a tool to study these aspects.

In the study of $^{9}$Be($^{7}$Li,$^{8}$Li)$^{8}$Be at $E_{\rm lab}$ = 2–4 MeV [16], it was observed that the principal mechanism is direct transfer of a neutron from the $^{9}$Be nucleus to the $^{7}$Li nucleus. It is expected that the reaction $^{7}$Li($^{7}$Li,$^{6}$He)$^{8}$Be will also be of the direct type and can proceed through the transfer of a proton. However, no clear confirmation of this argument has been provided in the earlier studies. The cross-sections of $^{6}$He channel obtained in $^{7}$Li + $^{7}$Li at energies of 3–4 MeV turned out to be small and the angular distributions were found to be almost isotropic or only slightly directed forward [17,18]. This reaction has also been studied at $E_{\rm lab}$ = 22 MeV, which is well above the Coulomb barrier [5], in which the measured angular distribution data for $^{6}$He was not explained satisfactorily by the DWBA calculations assuming one-step proton transfer. Further, $^{7}$Li can be considered as an alpha and triton cluster, which means that two-step processes like $^{7}$Li($^{7}$Li,$^{4}$He)$^{10}$Be ($^{4}$He,$^{8}$Be)$^{6}$He and $^{7}$Li($^{7}$Li,$^{4}$He)$^{10}$Be ($^{4}$He,$^{6}$He)$^{8}$Be are also possible, in addition to one-step proton transfer. Recently, Rosenthal *et al* [4] described various direct nuclear reaction channels in $^{7}$Li + $^{7}$Li at $E_{\rm lab}$ = 2–16 MeV. In that paper, it was concluded that the ($^{7}$Li,$^{6}$He) reaction proceeded predominantly as a direct proton transfer. With a motivation to understand the reaction mechanism of $^{6}$He production in $^{7}$Li($^{7}$Li,$^{6}$He) reaction in detail, measurements have been performed at two energies, $E_{\rm lab}$ = 20 and 25 MeV in the present work.

## 2. Experimental details

The experiment was performed using the $^{7}$Li beam at energies $E_{\rm lab}$ = 20 and 25 MeV, from the 14UD BARC-TIFR Pelletron accelerator, Mumbai. The target used was $^{\rm nat}$LiF of thickness ∼100 $\mu$g/cm$^2$, evaporated onto a carbon backing with a thickness of ∼50 $\mu$g/cm$^2$. Two telescopes ($\Delta E$–$E$) of silicon surface barrier (SSB) detectors were placed on one of the movable arms inside a 1 m diameter scattering chamber. The detector thicknesses were 50, 40, 1000 and 1500 $\mu$m for $\Delta$E1, $\Delta$E2, E1 and E2 detectors respectively. A monitor (single SSB of thickness 2000 $\mu$m) detector was fixed at 20° with respect to the beam direction for monitoring the beam quality and the variation in the target thickness when the target was rotated. The solid angles of both the telescopes were determined accurately by measuring the elastic (Rutherford) scattering from $^{209}$Bi target of known thickness. The beam intensity was measured using a precision current integrator. The angular distributions of charged particles were measured in the angular range of $\theta_{\rm lab}$ = 10° to 40°. In figure 1, the $^{6}$He spectrum measured at $\theta_{\rm lab}$ = 30° and $E_{\rm lab}$ = 25 MeV is shown. As can be seen from this figure, due to the presence of $^{19}$F in the target material, the $^{6}$He populating the 2$^+$, 3.04 MeV state of $^{8}$Be is merging with the $^{19}$F($^{7}$Li,$^{6}$He)$^{20}$Ne (2$^+$, 1.63 MeV state) and it could not be separated. This is true for data at all the measured angles. Hence, we have considered data corresponding to the transitions to the ground state only, for further analysis. The $^{12}$C($^{7}$Li,$^{6}$He)$^{13}$N reaction arising due to the $^{12}$C backing has relatively large negative $Q$ value ($Q$ = −8.032 MeV) and it does not appear in the region of spectra considered.

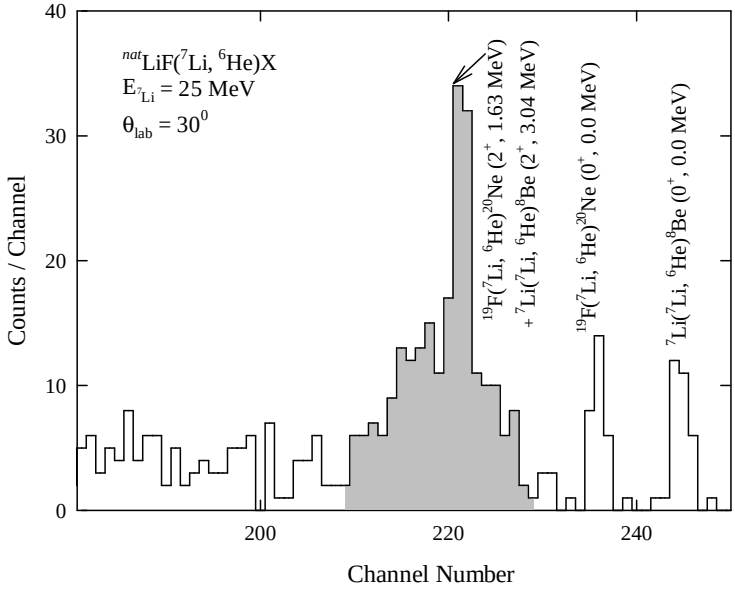


**Figure 1.** Measured energy spectra of $^6$He in $^7$Li+$^{nat}$LiF reaction at $\theta_{lab} = 30^\circ$, $E_{lab} = 25$ MeV. While the two peaks on right are clearly identified as due to $^7$Li($^7$Li,$^6$He)$^8$Be(g.s.) and $^{19}$F($^7$Li,$^6$He)$^{20}$Ne(g.s.), the shaded region shows the $^{19}$F($^7$Li,$^6$He)$^{20}$Ne ($2^+$, 1.63 MeV) state merging with a relatively broad $^7$Li($^7$Li,$^6$He)$^8$Be ($2^+$, 3.04 MeV) state.

As the target thickness was not precisely determined, the measured cross-sections at the forward-most angles ($\theta_{c.m.} \leq 20^\circ$) have been normalized to the optical model calculations. The calculations are found to be least sensitive to the choice of potential parameters in this angular region.

## 3. Results

### 3.1 *Elastic scattering angular distribution*

The measured elastic scattering angular distribution data were analysed using the optical model. There are a set of potentials available in the literature [6] for $^{6,7}$Li + $^{6,7}$Li systems for $E_{lab} = 5$–40 MeV. It is to be noted that these global potentials were tested for $^7$Li + $^7$Li system only for $E_{lab} = 8$–16 MeV. This is the first time that these potentials are tested for $E_{lab} = 20$ and 25 MeV.

All the optical model calculations were performed using the code 'FRESCO' [19] by taking into account the proper symmetrization due to the identical nature of target–projectile nuclei. From the set of potentials given in ref. [6], only a few potentials were found to fit the data satisfactorily. These potentials are listed in

**Table 1.** Optical model potential set taken from ref. [6] for $^7$Li + $^7$Li at $E_{\rm lab}$ = 20 and 25 MeV. The † sign is used to represent the depths of the potentials for 25 MeV. However, the geometrical parameters of the potentials are the same for both energies.

| Family | $V_0$ (MeV) | $r_{\rm R}$ (fm) | $a_{\rm R}$ (fm) | $W_{\rm S}/W_{\rm V}$ (MeV) | $r_{\rm I}$ (fm) | $a_{\rm I}$ (fm) | $r_{\rm c}$ (fm) |
|---|---|---|---|---|---|---|---|
| S-GL-2 | 4.0† | 0.994 | 1.467 | 3.7† | 1.467 | 0.473 | 1.25 |
| S-GL-3 | 4.9 | 1.234 | 1.618 | 11.9 | 1.246 | 0.534 | 1.25 |
| S-GL-5 | 16.7 | 0.562 | 1.557 | 12.1 | 1.232 | 0.567 | 1.25 |
| | 17.1† | | | 10.4† | | | |
| S-GL-6 | 28.7 | 0.122 | 1.752 | 13.4 | 1.197 | 0.591 | 1.25 |
| | 29.6† | | | 11.5† | | | |
| V-GL-1 | 7.3 | 1.086 | 1.310 | 6.3 | 1.651 | 0.311 | 1.25 |
| | 6.7† | | | 5.3† | | | |
| V-GL-2 | 18.9 | 0.612 | 1.434 | 6.6 | 1.636 | 0.345 | 1.25 |
| | 17.4† | | | 5.7† | | | |
| V-GL-3 | 34.0 | 0.173 | 1.617 | 7.9 | 1.589 | 0.397 | 1.25 |
| | 32.5† | | | 6.9† | | | |

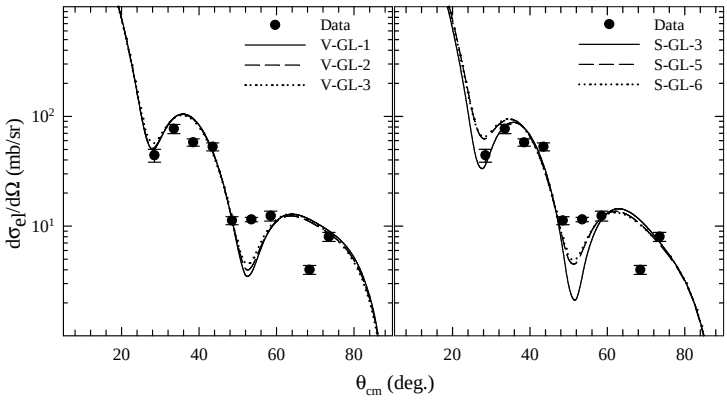


**Figure 2.** Elastic scattering angular distribution for $^7$Li + $^7$Li system at $E_{\rm lab}$ = 20 MeV. The lines indicate the optical model calculations using the potentials from ref. [6] (given in table 1).

table 1 . In figures 2 and 3 the measured elastic scattering angular distributions are shown along with the optical model calculations for 20 and 25 MeV respectively.

### 3.2 $^7Li(^7Li,^6He)$ *angular distribution*

#### 3.2.1 *One-step proton transfer*

In figure 4, the $^6$He angular distribution data corresponding to the population of $^8$Be (g.s., $0^+$, 0.0 MeV) is shown. The optical model potentials which described the elastic scattering data satisfactorily (shown in figures 2 and 3) were first used in

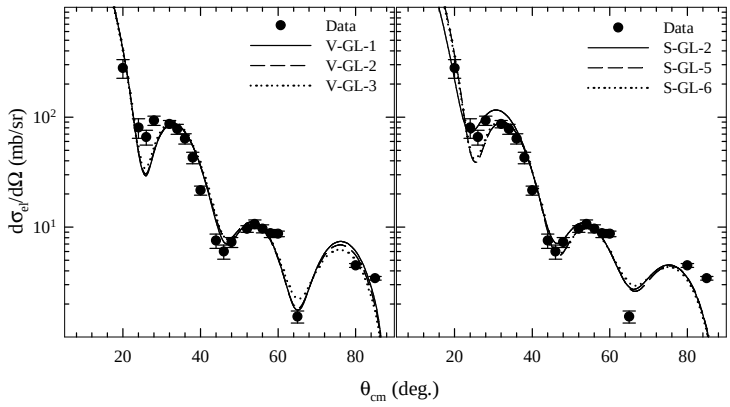


**Figure 3.** Same as figure 2 but for $E_{\rm lab} = 25$ MeV.

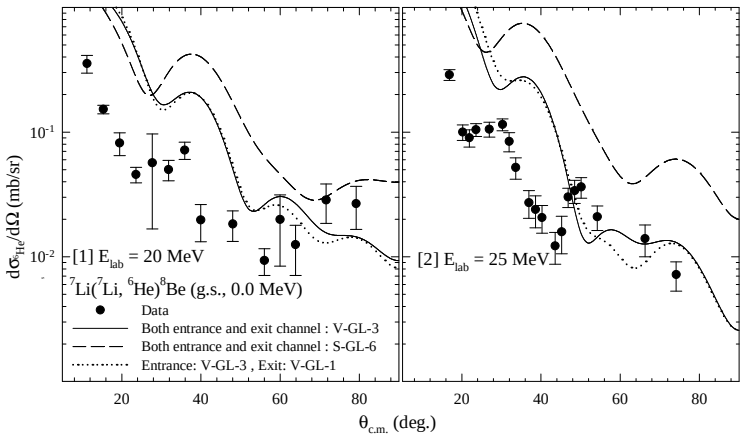


**Figure 4.** The measured $^6$He angular distribution data at $E_{\rm lab} = 20$ and 25 MeV are compared with predictions of the optical model for various entrance and exit channel potentials. See text for the details of the calculations.

the finite range DWBA (FRDWBA) calculations. All the FRDWBA calculations were carried out in post-formulation including the full complex remnant term. The potentials used to generate the $^7$Li $\rightarrow$ $^6$He + $p$ and $^8$Be $\rightarrow$ $^7$Li + $p$ bound states wave functions are adopted from ref. [4] and are given in table 2. To start with, same potentials for both the entrance ($^7$Li + $^7$Li) and the exit ($^6$He + $^8$Be) channels were used in the calculations. Two results (one from volume (V-GL-3) and other from surface (S-GL-6) absorption) are shown in figure 4 for both the measured energies. In addition, as suggested in ref. [4], we have used the deepest available potential (V-GL-3) for the entrance channel and the shallowest available potential (V-GL-1) for the exit channel (all potentials are provided in table 1). The results of these calculations for both the energies are shown in figure 4.

**Table 2.** New potential parameters used in FRESCO for calculations of elastic, one-step and two-step transfer angular distributions.

| System | $E_{\rm lab}$ (MeV) | $V_0$ (MeV) | $r_{\rm R}$ (fm) | $a_{\rm R}$ (fm) | $W_0$ (MeV) | $r_{\rm I}$ (fm) | $a_{\rm I}$ (fm) | $r_{\rm c}$ (fm) |
|---|---|---|---|---|---|---|---|---|
| *Optical model potentials* | | | | | | | | |
| $^{7}$Li + $^{7}$Li | 20 | 157.5 | 1.30 | 0.76 | 9.33 | 2.85 | 0.63 | 1.20 |
| (present work) | 25 | 157.8 | 1.22 | 0.75 | 10.46 | 2.81 | 0.63 | 1.20 |
| $^{6}$He + $^{8}$Be | 31.0 | 174.0 | 1.50 | 1.08 | 5.84 | 2.81 | 0.88 | 2.34 |
| (present work) | 34.6 | 174.0 | 1.56 | 0.88 | 5.84 | 2.81 | 0.88 | 2.34 |
| $^{4}$He + $^{12}$C | | | | | | | | |
| Ref. [22] | 41 | 199.1 | 1.26 | 0.65 | 42.17 | 1.26 | 0.65 | 1.25 |
| *Bound state potentials* | | | | | | | | |
| $^{6}$He + $p$ | – | a | 0.97 | 0.65 | | | | |
| $^{7}$Li + $p$ | – | a | 0.97 | 0.65 | | | | |
| $^{4}$He + $t$ | – | | | Gaussian form (ref. [23]) | | | | |
| $^{7}$Li + $t$ | – | a | 1.25 | 0.65 | | | | |
| $^{4}$He + $^{4}$He | – | a | 1.25 | 0.65 | | | | |
| $^{6}$He + $^{4}$He | – | a | 1.25 | 0.65 | | | | |
| $^{4}$He + 2$n$ | – | a | 1.25 | 0.65 | | | | |
| $^{8}$Be + 2$n$ | – | a | 1.25 | 0.65 | | | | |

The optical model potentials have the volume Woods–Saxon form with $R_x = r_x A_T^{1/3}$, where $x = c$ or $R$ or $I$.

The bound optical model potentials have a volume Woods–Saxon form with the geometrical parameters given in the above table. Here,

$$R_{\rm R} = r_{\rm R}(A_{\rm core}^{1/3} + A_{\rm cluster}^{1/3}).$$

[a]The depth ($V_0$) of bound state potentials were adjusted to give the correct separation energies.

As can be seen from figures 2–4 that, although the elastic scattering angular distribution data could be explained satisfactorily by the global set of parameters of ref. [6], the $^{6}$He angular distribution data could not be explained by using any combination of entrance and exit channel potentials listed in table 1. The calculated angular distribution differs significantly in the shape and the magnitude from the measured data. This propelled us to search for new entrance and exit channel potentials. We started with the potential parameters of $^{7}$Li + $^{9}$Be ($E_{\rm lab}$ = 24 MeV [20]) as initial parameters in search program of FRESCO [19] and searched for better potentials to explain the measured elastic scattering data (see table 2). For the required outgoing channel $^{6}$He + $^{8}$Be potentials, we have adopted the potentials of $^{6}$Li + $^{9}$Be ($E_{\rm lab}$ = 32 MeV) from ref. [21] as the starting set. These are also listed in table 2. The radius and diffuseness parameters of this exit channel potential have to be modified to reproduce the first dip in the $^{6}$He angular distribution data. The required orbital quantum numbers and the spectroscopic amplitudes ($\sqrt{C^2S}$) for the calculations were the same as those given in ref. [4]. In figure 5 both the elastic and one-step transfer calculations along with the data for two measured energies are

**Table 3.** Orbital quantum numbers $(N, L, J)$, binding energies (BE), and spectroscopic amplitudes ($\sqrt{C^2S}$) of the cluster bound states used in transfer calculations.

| Mechanism | Nucleus | Core | Cluster | BE (MeV) | $N$ | $L$ | $J$ | $\sqrt{C^2S}$ | Ref. |
|---|---|---|---|---|---|---|---|---|---|
| One-step | $^7Li_{g.s.}$ $(3/2^-)$ | $^6$He | $p$ | 9.975 | 1 | 1 | 3/2 | 0.77 | [24] |
| | $^8Be_{g.s.}$ $(0^+)$ | $^7$Li | $p$ | 17.255 | 1 | 1 | 3/2 | 1.00 | – |
| Two step | $^7Li_{g.s.}$ $(3/2^-)$ | $^4$He | $t$ | 2.467 | 2 | 1 | 3/2 | 1.084 | [4] |
| | $^{10}Be_{g.s.}$ $(0^+)$ | $^7$Li | $t$ | 17.251 | 2 | 1 | 3/2 | 0.556 | [4] |
| | $^{10}Be_{3.37}$ $(2^+)$ | $^7$Li | $t$ | 13.881 | 2 | 1 | 3/2 | 0.040 | [4] |
| | $^8Be_{g.s.}$ $(0^+)$ | $^4$He | $^4$He | $-0.092^*$ | 3 | 0 | 0 | 1.216 | [4] |
| | $^{10}Be_{g.s.}$ $(0^+)$ | $^6$He | $^4$He | 7.413 | 3 | 0 | 0 | 0.742 | [4] |
| | $^{10}Be_{3.37}$ $(2^+)$ | $^6$He | $^4$He | 4.043 | 3 | 0 | 0 | 0.721 | [4] |
| | $^6He_{g.s.}$ $(0^+)$ | $^4$He | $2n$ | 0.972 | 2 | 0 | 0 | 1.00 | – |
| | $^{10}Be_{g.s.}$ $(0^+)$ | $^8$Be | $2n$ | 8.477 | 2 | 0 | 0 | 1.00 | – |
| | $^{10}Be_{3.37}$ $(2^+)$ | $^8$Be | $2n$ | 5.107 | 2 | 0 | 0 | 1.00 | – |

*Instead of the negative BE, a very small BE = 0.009 MeV was used in the CRC calculation.

shown. A very good reproduction of both the elastic and transfer data confirmed the reliability of the optical model potentials employed and showed the dominance of one-step proton transfer for the description of this channel. It is interesting to note that the radius and diffuseness ($r_R$, $a_R$) parameter values obtained for the real potential of the $^6$He + $^8$Be (exit channel) are significantly larger than the ones found for $^7$Li + $^7$Li (entrance channel) system. This feature could be related to the large deformation (dumb bell shape) expected for the $^8$Be nucleus involved in the exit channel.

### 3.2.2 *Two-step transfer*

As mentioned in §1, in addition to one-step proton transfer, multistep processes for populating the $^6$He + $^8$Be channel are also possible. The sequential transfer paths of triton-$\alpha$ and triton-$2n$ transfers are shown schematically in figure 6. These two-step sequential transfer calculations were performed in the framework of the coupled reaction channels (CRC) method using the code FRESCO. The prior and post-interactions were used for the first and second steps of the sequential transfers, respectively. Apart from the potentials used in one-step proton transfer, additional potential for the intermediate state $^4$He+$^{10}$Be was required. It was taken as the same as that of $^4$He+$^{12}$C from ref. [22]. Also the required binding potentials are given in table 2. These two-step transfer calculations corresponding to the transfer steps shown schematically in figures 6A and 6B, were performed for two measured energies and results are shown in figure 7. The quantum numbers and spectroscopic amplitudes ($\sqrt{C^2S}$) used in the two-step calculations are given in table 3. Due to the lack of knowledge about the reliable cluster spectroscopic amplitudes and the binding potentials, the absolute magnitude of the two-step transfers are uncertain

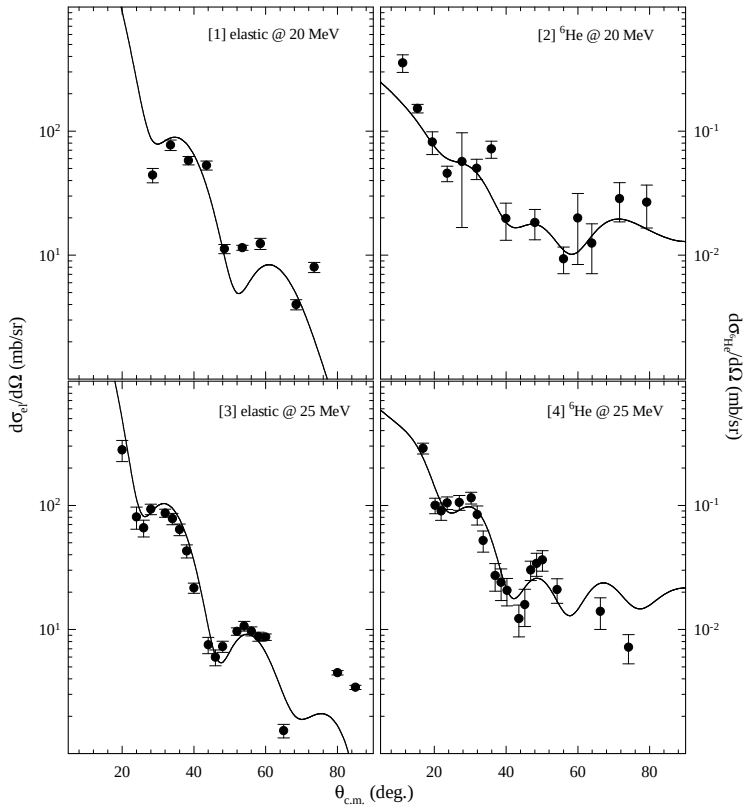


**Figure 5.** Both elastic and $^{6}$He angular distribution data at two measured energies are compared with the FRESCO (elastic and one-step proton transfer) calculations by using the new set of potentials given in table 2.

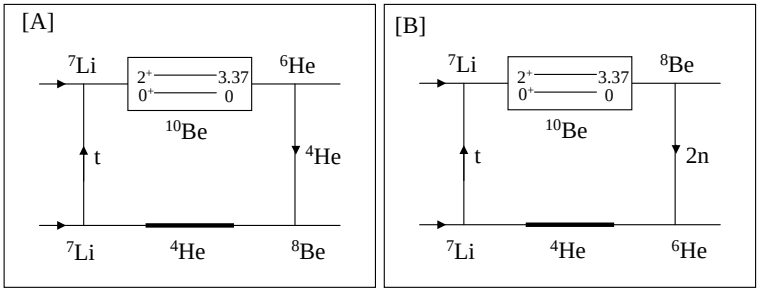


**Figure 6.** Schematics of two-step transfer calculation populating $^{6}$He + $^{8}$Be channel. Two possibilities considered are shown in (**A**) and (**B**).

and have been renormalized by a factor of 40 and 35 for the cases shown in figures 6A and 6B respectively. In figure 7 a comparison is made between one-step proton transfer and two-step transfer calculations. As can be seen from the figure, the

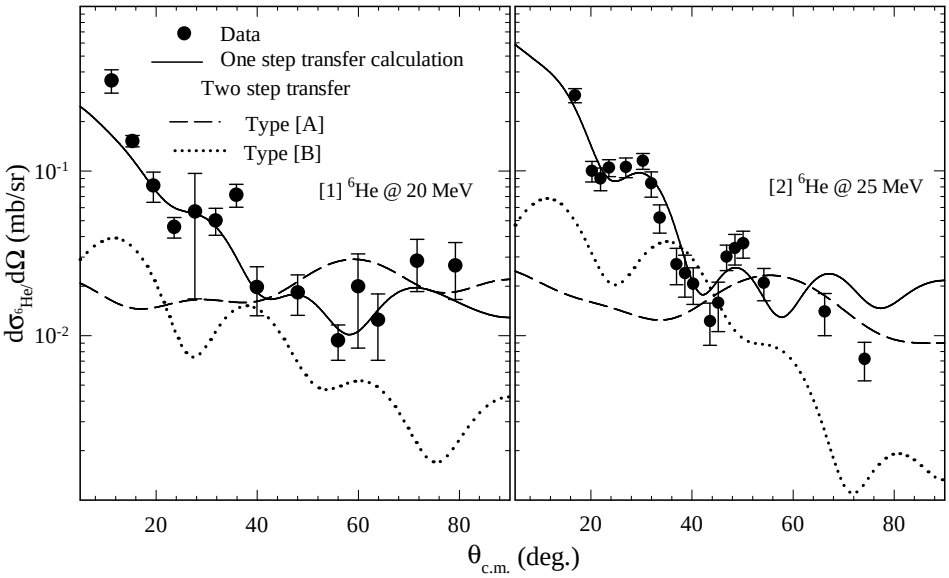


**Figure 7.** The $^6$He angular distribution data at two measured energies is shown along with one-step transfer and two-step transfer calculations of figures 6A and 6B. See text for details.

one-step and two-step calculations corresponding to $t$-$\alpha$ sequential transfer are in good agreement at larger angles $\theta \geq 50°$. On the other hand, two-step $t$-$2n$ sequential transfer shows a large discrepancy in shape with the measured data. Angular distribution data at larger angles are very much required in order to draw any definite conclusions on these aspects. From the present data it is clear that the measured angular distributions are consistent with the dominant one-proton transfer process.

## 4. Summary

In summary, the $^7$Li($^7$Li,$^7$Li) and $^7$Li($^7$Li,$^6$He) angular distributions have been measured at $E_{\rm lab}$ = 20 and 25 MeV. Various optical model potentials of ref. [6] have been examined for describing the measured elastic scattering angular distribution data. It was found that although some of the global potentials of ref. [6] reproduce the elastic scattering angular distribution reasonably well, they fail to explain the $^6$He angular distribution data. The new potentials determined in the present work for the entrance and the exit channels could reproduce both the elastic and $^6$He angular distribution data well. This suggests that, there exists a strong dependence of the FRDWBA angular distribution on the used optical model potentials. The contribution from one-step transfer is found to be the dominant one for the description of $^7$Li($^7$Li,$^6$He) reaction. The two-step sequential transfer is very weak and the small effect due to this process is seen at backward angles.

**Acknowledgments**

The authors would like to thank the Pelletron crew for the smooth operation of the accelerator during the experiments and to Mr Mahadkar and Mrs Deepa for target preparations. The help during the experiment from Mr P Patale is gratefully acknowledged. We would like to acknowledge the suggestions from Prof. B. Kamys which helped in improving the calculations. One of the authors (VVP) acknowledges the financial support of Department of Atomic Energy, Government of India, in carrying out these investigations.

**References**

[1] Y Leifels, G Domogala, R P Eule and H Freiesleben, *Z. Phys.* **A335**, 183 (1990)
[2] G Domogala and H Freiesleben, *Nucl. Phys.* **A467**, 149 (1987)
[3] S Adhikari, C Samanta, C Basu, B J Roy, S Ray, A Shrivastava, K Ramachandran, V Tripathi, K Mahata, V Jha, P Shukla, S Rahi, M Biswas, P Roy Chowdhury, A Chatterjee and S Kailas, *Phys. Rev.* **C74**, 024602 (2006)
[4] P Rosenthal, H Freiesleben, B Gehrmann, I Gotzhein, K W Potthast, B Kamys and Z Rudy, arXiv:0801.2264v1 [nucl-ex] (2008)
[5] O V Bochkarev, A A Korsheninnikov, E A Kuźmin, I G Mukha, L V Chulkov and G B Yańkov, *Yad. Fiz.* **47**, 616 (1988); [*Sov. J. Nucl. Phys.* **47**, 391 (1988)]
[6] K W Potthast, H Brand, H Freiesleben, P Rosenthal, B Kamys, H Paetz gen Schieck and L Sydow, *Nucl. Phys.* **A614**, 95 (1997)
[7] E A Benjamim, A Lepine-Szily, D R Mendes, Jr, R Lichtenthaler, V Guimaraes, P R S Gomes, L C Chamon, M S Hussein, A M Moro, A Arazi, I Padron, J Alcantara Nunez, M Assuncao, A Barioni, O Camargo, Jr, R Z Denke, P N de Faria and K C C Pires, *Phys. Lett.* **B647**, 30 (2007)
[8] J J Kolata, H Amro, F D Becchetti, J A Brown, P A DeYoung, M Hencheck, J D Hinnefeld, G F Peaslee, A L Fritsch, C Hall, U Khadka, Patrick J Mears, P O'Rourke, D Padilla, J Rieth, T Spencer and T Williams, *Phys. Rev.* **C75**, 031302 (2007)
[9] O R Kakuee, M A G Alvarez, M V Andres, S Cherubini, T Davinson, A Di Pietro, W Galster, J Gomez-Camacho, A M Laird, M Lamehi-Rachti, I Martel, A M Moro, J Rahighi, A M Sanchez-Benitez, A C Shotter, W B Smith, J Vervier and P J Woods, *Nucl. Phys.* **A765**, 294 (2006)
[10] M Milin, S Cherubini, T Davinson, A Di Pietro, P Figuera, D Miljanic, A Musumarra, A Ninane, A N Ostrowski, M G Pellegriti, A C Shotter, N Soic, C Spitaleri and M Zadro, *Phys. Atomic Nuclei* **69**, 1360 (2006)
[11] R L White and K W Kemper, *Phys. Rev.* **C10**, 1372 (1974)
[12] A F Zeller, K W Kemper, T R Ophel, D C Weisser, D F Hebbard, A Johnston and G T Hickey, *Nucl. Phys.* **A309**, 255 (1978)
[13] K W Kemper, A F Zeller, T R Ophel and D P Stanley, *Nucl. Phys.* **A391**, 237 (1982)
[14] G H Neuschaefer, M N Stephens, S L Tabor and K W Kemper, *Phys. Rev.* **C28**, 1594 (1983)
[15] K Ioannides, P Assimakopoulos, A Pakou and S Kossionides, *Z. Phys.* **A321**, 225 (1985)
[16] E Norbeck, J M Blair, L Pinsonneault and R J Gerbracht, *Phys. Rev.* **116**, 1560 (1959)

[17] Robert A Stryk and J M Blair, *Phys. Rev.* **169**, 767 (1968)
[18] R R Carlson, R L McGrath and E Norbeck, *Phys. Rev.* **136**, B1687 (1964)
[19] I J Thompson, *Comput. Phys. Rep.* **7**, 167 (1988)
[20] J Cook, *At. Data Nucl. Data Tables* **26**, 19 (1981)
[21] J Cook and K W Kemper, *Phys. Rev.* **C31**, 1745 (1985)
[22] C M Perey and F G Perey, *At. Data Nucl. Data Tables* **17**, 1 (1976)
[23] B Buck and A C Merchant, *J. Phys. G: Nucl. Phys.* **14**, L211 (1988)
[24] S Cohen and D Kurath, *Nucl. Phys.* **A101**, 1 (1967)